Available online at www.sciencedirect.com

SciVerse ScienceDirect

Journal of the European Ceramic Society 32 (2012) 2193–2201

www.elsevier.com/locate/jeurceramsoc

# Potentials of the "Direct inkjet printing" method for manufacturing 3Y-TZP based dental restorations

Emre Özkol *, Wen Zhang, Jörg Ebert, Rainer Telle

*Department of Ceramics and Refractory Materials, RWTH Aachen University, Mauerstraße 5, D-52064 Aachen, Germany*

Received 18 July 2011; received in revised form 19 December 2011; accepted 1 March 2012
Available online 20 March 2012

**Abstract**

The potentials of the direct inkjet printing (DIP) method for manufacturing 3Y-TZP dental restorations were investigated. Aqueous inks of 3Y-TZP and carbon were developed and characterised for the DIP method. A sample 3Y-TZP framework of a dental bridge was produced by DIP. The stress distribution on this framework under realistic clenching conditions was simulated using finite element analysis. Four-point bending specimens produced by DIP and a slip cast reference sample were tested to characterise the flexural strength of the DIP produced components.


*Keywords:* Direct inkjet printing; $ZrO_2$; Mechanical properties; Strength; Biomedical applications

## 1. Introduction

Engineering oxide ceramics have become increasingly popular in dental prosthetics because of their biocompatibility, low bacterial adhesion, enhanced aesthetics, match to traditional cementation procedures as well as excellent mechanical properties and wear resistance.[1–6] In addition, zirconia ceramics especially the 3Y-TZP (3 mol.% $Y_2O_3$ stabilised tetragonal zirconia polycrystals) reveal a superior fracture toughness, which is given by the material-specific transformation toughening mechanism.[5–8] The excellent mechanical properties of 3Y-TZP distinguish this material as a perfect candidate for dental restorations. However, manufacturing such ceramic dental components, which are usually of relative complex geometry, is not trivial.

The requirements of the manufacturability of 3Y-TZP dental restorations were successfully fulfilled after the introduction of computer-aided design and computer-aided manufacturing (CAD/CAM) technology to the field of restorative dentistry.[3,9–11] Currently, two main methods exist, which apply the CAD/CAM technology to produce such components. The first method is basically a hard machining process of fully sintered ceramic blocks in order to produce dental frameworks made of zirconia (e.g. DC-Zirkon®/DCS Dental AG, Denzir®/Cadesthetics AB).[6,12,13] The other method can be defined as a soft machining process of partially sintered porous ceramic blocks, which are subsequently sintered in order to produce the final components (e.g. Cercon®/Dentsply International, Lava™/3M™ ESPE™, Procera® zirconia/Nobel Biocare™, YZ cubes for Cerec InLab®/Vident™, IPS e.max® ZirCAD/Ivoclar Vivadent).[6,12,13] Both methods are based on a subtractive milling process, which results in a considerable amount of wasted valuable raw material. Furthermore, both methods require a ceramic pre-form as an input for the CAD/CAM equipment.[1,9] These pre-forms must reveal certain characteristics in terms of uniformity, compaction density, and robustness in order to be successfully machined at the CAD/CAM system. Moreover, the pre-forms must be carefully stored and shipped before and after the milling operation.[14] Considering the production and handling of the pre-form material increases the number of the process parameters as well as the total complexity of the CAD/CAM methods used to manufacture dental restorations. A complex process is not very suitable to produce dental restorations, which must reveal a relative high level of reliability once implanted in the oral environment.

On the other hand, additive (generative) manufacturing techniques have the potential to produce components of complex shape and composition in a fast, accurate, and direct way, while minimising the wasted material.[15–17] These techniques generate small modular units of the building material and build the component by bringing these units together. Some

* Corresponding author. Tel.: +49 2418094981; fax: +49 2418092226.
*E-mail address:* oezkol@ghi.rwth-aachen.de (E. Özkol).

0955-2219/$ – see front matter © 2012 Elsevier Ltd. All rights reserved.
doi:10.1016/j.jeurceramsoc.2012.03.006

of the most commonly used methods for producing ceramic components are stereolithography,[18] robocasting,[19–22] selective laser sintering,[23] laminated object manufacturing,[24] three-dimensional printing,[25,26] and direct inkjet printing (DIP).[27–30] So far only few studies were reported for fabricating dental restorations with DIP[14] and robocasting[19,20] methods.

DIP can be described as the layer-wise deposition of particle loaded droplets to build a three-dimensional object using an ink deposition nozzle.[27–30] Robocasting is a similar method but it uses extruded filaments instead of ejected droplets to evolve an object.[19–22] Both techniques are computer controlled and require only a substrate as a base for the deposition. Although they are both theoretically capable of achieving[22] the commercial surface requirements of 20–50 μm[20] and marginal accuracy of ∼100 μm[12] for dental restorations the DIP technique offers a better shape accuracy due to the smaller sized droplets (in this case $35 \times 10^{-12}$ L)[31,32] compared to the typical filament sizes larger than 100 μm in robocasting.[19–22] Besides among the above mentioned additive techniques DIP is the only method, which can be used to produce ceramic components of full density (low porosity)[30,31] and good mechanical properties.[32,33] In addition a graded composition throughout the component[33,34] as well as cavities inside the component[35] can be realised. All these aspects would make DIP a promising and interesting fabrication method for manufacturing individually shaped, accurate, high strength, ceramic components of complex geometry. These characteristics of printed objects are quite the same of the requirements of ceramic dental restorations.

The objective of this study is to show the potentials of DIP for producing zirconia based dental restorations. For this purpose the following three questions have to be answered. Is the DIP method capable of fabricating dental restorations using virtual computer models? What are the stresses acting on the dental restorations during realistic clenching conditions? Are DIP-fabricated dental restorations reliable under the computed stresses? This study answers these questions in three sections. In the first section the DIP-fabrication steps of a 3Y-TZP dental bridge framework are described. Here the preparation as well as the characterisation of the ceramic ink and the details of the DIP method is explained. The second section introduces an FE-analysis, which computes the stress distribution as well as the maximum tensile stress on the framework model under realistic clenching conditions. The FE-analysis defines the strength requirements of the materials, which can be used to build the framework. In the third section the characteristic strength of the DIP-fabricated 3Y-TZP components are determined by a four-point bending test.

## 2. Experimental procedure

### 2.1. Materials and ink characteristics

Ceramic and supportive inks were separately prepared and printed. The ceramic ink was an aqueous dispersion of submicron sized (mean particle diameter of 0.63 μm) 3Y-TZP particles (TZ-3YS-E, Tosoh Inc., Japan). A carboxylic acid based dispersant (Dolapix CE64, Z&S Inc., Germany) was used. A suspension of 40 vol.% solids content and 0.5 wt.% (related to solids) dispersant was attrition milled at 1200 rpm for 30 min. The slip cast specimens were prepared using this suspension. The suspension was diluted to 27 vol.% solids content to prepare the ceramic ink by addition of water, dispersants, and humectants in order to reduce the viscosity and adjust the drop ejection behaviour. The dispersant content was set as 1 wt.% (related to solids). Polyols were used as humectants and the content in the final ink was ∼25 vol.% (related to the liquid phase). The solidification of the ceramic ink was provided by the evaporation of the liquid phase. Several studies used waxes as binders.[27,28] The ink did not contain any wax-based binders. A detailed description of the ink synthesis is given elsewhere.[14,31]

The supportive ink was an aqueous dispersion of sub micron sized (average primary particle size of 0.28 μm) thermal black type carbon black particles (Arosperse® 15, Evonik Chemicals, Germany). An alkali free carboxylic acid ester based dispersant was used (Dolapix ET85, Z&S Inc., Germany). The ink was ball milled for 36 h using $Al_2O_3$ beads of 5 mm diameter prior to jetting.

Both of the inks were characterised in terms of viscosity and surface tension at 20 °C. A rotational rheometer (Viscolab LC10, Physica, Germany) with a double gap concentric measuring system was used to determine the viscosity at a shear rate of 1000 $s^{-1}$. The surface tension of the inks was measured according to the bubble pressure method (Proline t15, Sita Corp., Germany) for a bubble lifetime of 0.5 s.

The jetting behaviour of the inkjet inks can be summarised by the dimensionless Ohnesorge number ($Oh$), which can be calculated using the physical ink properties:

$$Oh^{-1} = \frac{(\sigma \cdot \rho \cdot a)^{1/2}}{\eta} \quad (1)$$

where $\sigma$ is the surface tension, $\rho$ is the density, $a$ is a characteristic length (the nozzle radius), and $\eta$ is the viscosity of the ink. The suitable region for stable jetting is defined as $1 < Oh^{-1} < 10$.[28,36] This $Oh^{-1}$ number was calculated for both of the inks and the values were compared to the previously published results.

### 2.2. Direct inkjet printing (DIP) of the components

A modified office-type thermal inkjet printer (HP Deskjet 930c®) was used to jet the inks using the black ink cartridge (HP51645A). The modifications basically provided an overwriting in order to realise the production of a three-dimensional components. The printhead moves only in the $x$ direction and covers a width of ∼12 mm when all nozzles are fired at the same time, which limits the $y$ dimension of the printable area by ∼12 mm. Therefore it was not possible to produce the bridge framework in original size and the framework was downscaled to the limits of the printing station. Further details of the printing station and procedure are given elsewhere.[32,33]

Before starting the printing process, a complete set of the two-dimensional cross section data of the three-dimensional model must be generated and transmitted to the printer. In order to produce the bending specimens a black coloured (RGB: 0/0/0)

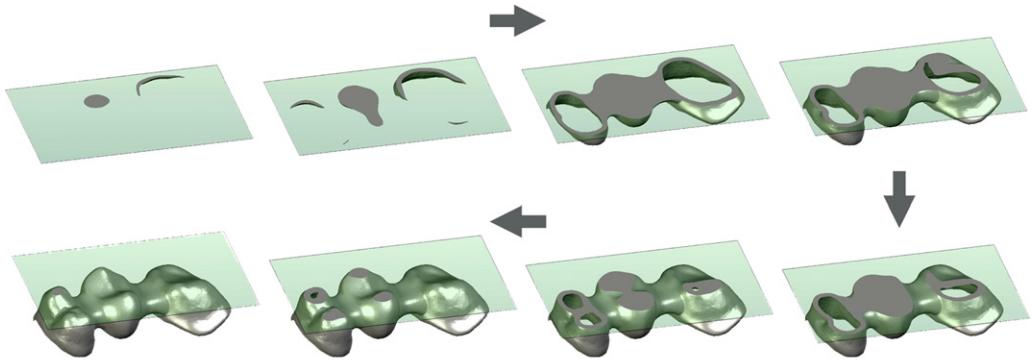

Fig. 1. Visualisation of the layer-wise production stages of the printed demonstration object.

rectangle was used as the input cross-section data and this figure was over-printed onto a graphite substrate (SGL Carbon, Germany).

In case of the framework structure, the cross-section varies throughout the object as shown in Fig. 1. Therefore it is necessary to generate a two-dimensional dataset (e.g. an image to be printed) of each cross-section individually. The dataset of all cross-sections was generated by slicing the three-dimensional model of the framework (Fig. 1) using a special software. The thickness of the slices was set as 5 μm. The framework structure has a complex shape (Fig. 1), which contains overhanging features in all directions. It is not possible to print such an object onto a flat substrate. Therefore the substrate surface was modified by printing a base made of supportive material on the flat substrate and the framework was printed onto this base. In this manner the top and bottom topographies of the framework were successfully realised. The cross-sectional data of the base was generated by the special software for a layer thickness of 3 μm.

The printed components were dried at room temperature after printing and were stored 12 h at 80 °C. The storage in the drying cabinet ensured that almost all of the residual humidity as well as humectants were removed. The organic residues were removed by a 3 h heat treatment at 550 °C. Another heat treatment for 3 h at 850 °C was applied in order to separate the supportive structure as well as the substrates from the components. Finally the components were 2.5 h sintered in a coarse $ZrO_2$ powder bed at 1450 °C.

### 2.3. Finite element analysis (FEA)

Finite element analysis (FEA) was performed to investigate the stress distributions inside the framework structure. In the FE-model, the framework structure was loaded according to the occlusal clenching forces reported by other studies.[37,38] Various loading conditions were considered to compute the maximum tensile stresses on the framework under different loading situations.

#### 2.3.1. Finite element model

The model of the bridge framework was generated from an STL file (Fig. 1). The other two support models to represent

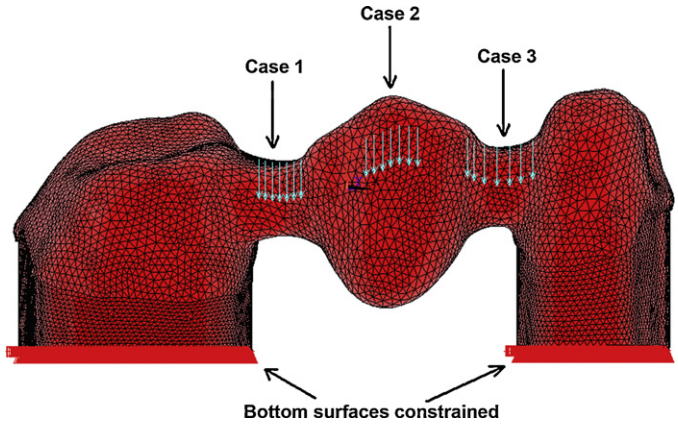


Fig. 2. The FE-model and the three different cases showing the location of the applied forces.

the restored 1st premolar and 1st molar were created using an FE pre-processor (Altair® HyperMesh® v. 9.0) by filling the cavities at the two ends of the framework structure (Fig. 2). Therefore, no interlayer was simulated between the framework and the restored teeth. These three models were defined individually as three components and separately exported as input files in engineering simulation software (ANSYS® v. 11.0) after meshing in the pre-processor. FEA was performed using ANSYS® Classic afterwards. All materials were assumed to be homogeneous, isotropic, and linear elastic in the range of the applied loads that were chosen for the finite element calculations. The material properties used in the FEA models were given in Table 1.[39,40] The interfaces between the bridge framework and the restored 1st premolar and 1st molar were assumed to be perfectly 'bonded'. This simplification was considered to be reasonable, since in the practice they were all fully glued by a thin layer of an adhesive material.[41]

Table 1
Material properties used in the FE models.[39,40]

| Material | Young's modulus, $E$ [GPa] | Poisson's ratio, $\nu$ |
|---|---|---|
| $ZrO_2$ (Bridge framework) | 200 | 0.27 |
| Restored teeth | 20 | 0.3 |

8-Nodes hexahedral finite element SOLID 45 was selected. The framework model possessed 51,667 elements, whereas the restored 1st premolar and 1st molar model were of 33,815 elements and 47,554 elements, respectively.

#### 2.3.2. Loading and boundary conditions

A common loading situation was adopted. Previous studies reported clenching occlusal forces of about 350–475 N for molar elements and about 60–290 N for premolar elements.[37,38] The bridge framework model includes both premolar and molar units. Therefore it was decided to load the model according to an occlusal force for the molar region. The loading force was further extended with three times of the standard deviation in order to cover a realistic range of occlusal force during clenching. The force applied was calculated to be ~850 N, which is comparable to the maximum clenching forces given in similar studies.[4,7,9,11]

The force was equally distributed on 7 representative neighbouring nodes and was applied in the negative $z$ direction assuming three different cases (Fig. 2): (1) On the connector between the 1st molar and the 2nd premolar units of the bridge model, (2) On the 2nd premolar unit, (c) On the connector between the 1st premolar and 2nd premolar units of the bridge model. 7 neighbouring nodes were carefully selected from the central pontic area of each bridge unit. The force was applied on those 7 neighbouring nodes in order to simulate a situation where a punctual force (e.g. a small and hard solid particle) would cause a maximum pressure on the framework. The bottom surfaces of the support models were fully constrained during loading.

### 2.4. Mechanical testing and evaluation of the strength

The fracture strength of the inkjet printed and slip cast specimens was determined using a four-point bending setup. A universal testing machine (model 1186H0425, Instron, Germany) was used and a stressing rate of 100 MPa $s^{-1}$ was applied. The respective inner and outer roller spans were 12 and 24 mm.

The surfaces of the bending specimens were ground on a precision surface grinding machine (PS R300, G&N, Germany). The respective sample sizes of the tested inkjet printed and slip cast specimens was 34 and 10. The approximate dimensions of the inkjet printed and slip cast bars were 1.5 mm × 3.0 mm × 30.0 mm and 3.5 mm × 4.2 mm × 52.5 mm, respectively.

Weibull statistics are typically used to describe the strength characteristics of ceramic materials.[32,43,44] A regression analysis was performed using the Minitab 16 statistical software to fit the Weibull modulus (shape parameter) and the characteristic strength (scale parameter) of the two-parameter Weibull distribution using the experimental fracture stress data. The maximum likelihood estimation was used. The two-parameter Weibull distribution of failure probability, $F$, is given by:

$$F(\sigma) = 1 - \exp\left(\frac{-\sigma}{\sigma_0}\right)^m \quad (2)$$

where $\sigma$ is the fracture stress, $\sigma_0$ is the characteristic strength at the fracture probability of ~63.2%, and $m$ is the Weibull modulus.[43]

The strength values of the two samples cannot be directly compared with each other because of the different specimen dimensions, which define the effective volume under load in the bending test.[43,44] The effective volume, $V_{eff}$, is defined as the volume of a theoretical specimen, which has the same fracture probability as the whole specimen when subjected to the fracture stress.[44] The effective volume for a four-point bending setup, where the distance between each inner and outer support is equal to the 1/4th of the outer roller span (also equal to the half of the inner roller span), is given by:

$$V_{eff} = \left(\frac{V_{test}}{4}\right) \cdot \frac{(m+2)}{(m+1)^2} \quad (3)$$

where $V_{test}$ is the volume within the outer support points.[44]

Knowing that both samples were tested by the four-point bending test and the fracture was due to tensile stress, the following equation can be used to scale and compare the characteristic strength of the DIP and slip cast samples with different specimen sizes:

$$\sigma_{0,1} = \sigma_{0,2} \cdot \left(\frac{V_{eff,2}}{V_{eff,1}}\right)^{1/m} \quad (4)$$

where $\sigma_{0,1}$ and $\sigma_{0,1}$ are the respective characteristic strengths of the samples and $V_{eff,1}$ and $V_{eff,2}$ are the respective effective volumes of the specimens.[43,44]

## 3. Results and discussion

### 3.1. Characterisation of the inks

Both of the ceramic and carbon black inks were jettable using the printing device. Mechanical clogging of the nozzles or internal feed-channels of the printhead due to solid particles or agglomerates was not observed.

The viscosity values of the ceramic and supportive inks were determined to be ~15 mPa s and ~4 mPa s, respectively. The viscosity of the ceramic ink was comparably high considering the values obtained in previous studies.[31,42] This difference is because of the 3 vol.% increase in the solid content of the current ceramic ink. Similarly the lower viscosity of the supportive ink can be explained by the lower solid content of the ink.

The surface tension of the ceramic and supportive inks was measured as ~42 mN $m^{-1}$ and ~38 mN $m^{-1}$, respectively. The density of the ceramic ink was 2.35 g $cm^{-3}$ while the supportive ink had a density of 1.06 g $cm^{-3}$.

These ink properties were used to calculate the dimensionless $Oh^{-1}$ number of the inks. This number is a general indicator of the printability for any type of ink. The respective $Oh^{-1}$ numbers of the ceramic and supportive inks were determined as ~2.5 and ~6. Both of these values are in the range of printability, which is given as $1 < Oh^{-1} < 10$. The comparatively high density and viscosity of the ceramic ink explains the lower $Oh^{-1}$ number. Although the inks are classified as printable, the integrity of

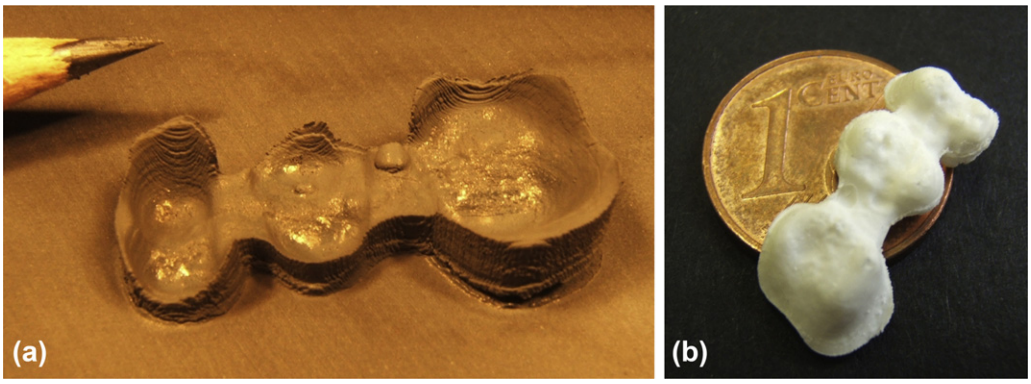


Fig. 3. Produced by DIP: (a) the supportive base made of carbon black and (b) the 3Y-TZP bridge framework (sintered).

the jetted droplets cannot be definitely concluded according to the $Oh^{-1}$ number. Previous studies using inkjet printers with thermal activation showed poor agreement with the upper limit of the $Oh^{-1}$ number and drop integrity.[32,42]

### 3.2. Evaluation of the direct inkjet printed (DIP) components

A downscaled 3Y-TZP bridge framework as well as bending specimens ($n = 34$) were successfully manufactured by DIP. In previous work, the high accuracy and precision of printed delicate structures[14,42] was investigated but a component on cm-scale such as the framework structure was not introduced until this study. The carbon base (Fig. 3a) as well as the 3Y-TZP framework (Fig. 3b) are unique examples showing the manufacturability of components in millimetre scale by DIP. Moreover the printed components did reveal neither stair steps on the surface nor drying and sintering cracks.

The printing unit is equipped with a single black ink cartridge. Therefore the cartridge was first filled with the supportive ink and the base was completely built. Afterwards another cartridge filled with the ceramic ink was placed and the framework was printed onto the base. Therefore the optimum distance between the printhead and substrate surface could not be maintained in case of printing the ceramic ink. The larger the distance the longer is the period of the droplet flight time. This would mislead the position of the drop impact on the substrate and therefore reduces the accuracy of the printed structure.

On the other hand the distance between the printhead and the substrate was optimum as the supportive base was printed. Therefore the base is in general more precisely fabricated. In order to increase the accuracy of the framework structure on the occlusal side, the supportive structure was designed to support the occlusal side (upper side in Fig. 3b) of the framework and the framework was printed upside down onto the base. In this manner, the accuracy of the base was transferred to the upper surface of the framework. However the carbon structure in Fig. 3a reveals a defect, which is a spot higher than the surrounding, located on the interconnector on the right side. The framework model (Fig. 1) does not reveal such a void at this position and thus the defect is related to the DIP process. The origin of the defect may be a contaminating particle, which interfered the fabrication process (e.g. a piece of textile fibre), or a bubble formed in the lower layers during drying. This object or bubble was covered with ink during subsequent deposition resulting in the spot in Fig. 3a. The defect on the base was transferred to the framework structure forming a void on the top surface as shown in Fig. 3b.

Both carbon and ceramic inks were aqueous based and therefore miscible with each other. Therefore a risk of mixing of both inks would be present in case of a simultaneous deposition using multi-printhead systems. However in this specific case the base was deposited and dried completely before the ceramic was deposited onto it. As a result no mixing of the both phases was observed.

In addition, the relative density of the sintered framework structure was determined according to the Archimedes' principle. The density was $\sim 5.82\,g\,cm^{-3}$, which is >96% of the theoretical density.

As mentioned before dental restorations were fabricated using the DIP[14] and robocasting[19,20] methods among the typical additive manufacturing techniques. A comparable dental bridge framework structure made of zirconia was also fabricated with the robocasting method.[19] The solid content of the pastes used in robocasting were higher than in the DIP inks but the amount of organic additives in the deposited components were in a comparable range.[19,22] Despite the higher solid content of the paste the framework structure fabricated by robocasting was not totally free of cracks.[19] This could indicate that the drying of layers of droplets is more effective than extruded filaments suppressing the formation of drying cracks. Moreover the components fabricated by robocasting revealed stair steps on the surface[19,20,22] whereas the surface was comparably smooth in case of the DIP fabricated framework.

### 3.3. Results of the FE-analysis

In the FE simulation, the first principal stress on the framework structure was examined. The stress distribution and the maximum tensile stress under the three different loading situations (cases 1–3 in Fig. 2) were computed and shown in Fig. 4. The results of all different loading cases show hot spots on the bottom marginal area of the interdental connectors. The respective maximum tensile stress values are

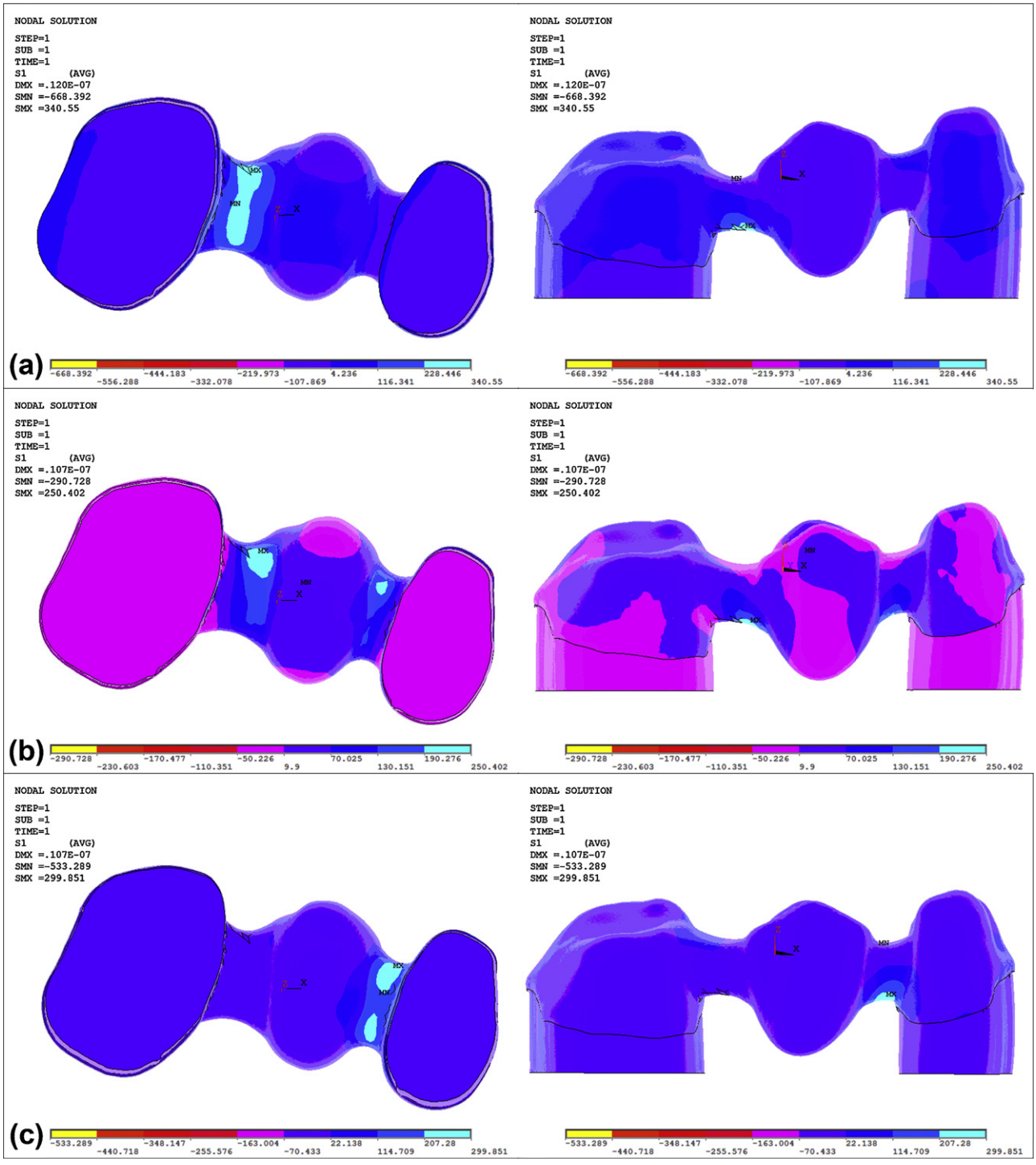


Fig. 4. Results of the FE simulation showing the stress distribution on the framework (bottom and side view) for (a) case 1, (b) case 2, and (c) case 3 loading conditions.

predicted to be ∼340 MPa and ∼300 MPa for cases 1 and 3, where the occlusal force is applied onto the connector. In both cases the hot spot is below the connector, on which the force is applied. In case 2, the maximum tensile stress is ∼250 MPa and hot spots are located below both connectors.

The goal of this FE simulation was to determine a rough but realistic estimate of the stress distribution on a dental framework structure under usual clenching conditions. Therefore a realistic maximum occlusal force was applied onto a real framework model. Moreover, to simulate a worst case scenario (impact of a small and hard solid particle) the total force was located on

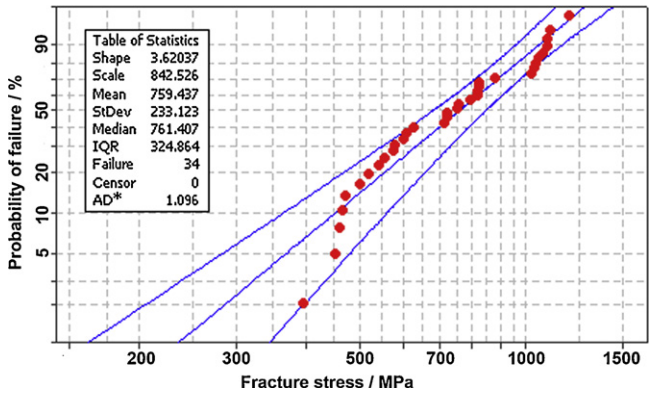


Fig. 5. Fracture stress vs. probability of failure diagram showing the distribution of the fracture strength of DIP specimens.

a small area on the framework. Although several factors in an in vivo occlusal loading environment were excluded in order to simplify the FE model and calculations, the predicted values of the maximum tensile stress were in good agreement with similar studies.[9,11]

### 3.4. Flexural strength of DIP and slip cast specimens

The mechanical properties of ceramic materials are described by a statistical distribution depending on the composition and grain size of the material as well as the manufacturing process.[43,44] Any change in the production process would influence the strength of a ceramic component of the same composition and shape. Under optimum processing conditions, the 3Y-TZP material can achieve a flexural strength up to 1500 MPa.[43]

In order to determine the flexural strength of the 3Y-TZP components produced by DIP, bending specimens were produced and tested. Fig. 5 shows the probability of failure diagram of the DIP specimens assuming a Weibull distribution for the fracture stress. The characteristic strength was determined as $\sigma_{0,DIP} = \sim 843$ MPa (scale parameter in Fig. 5) with a 95% confidence interval of [764–930]. The fracture stress values of the specimens varied between ~400 and ~1200 MPa, corresponding to a Weibull modulus $m_{DIP} = 3.6$ (scale parameter in Fig. 5)

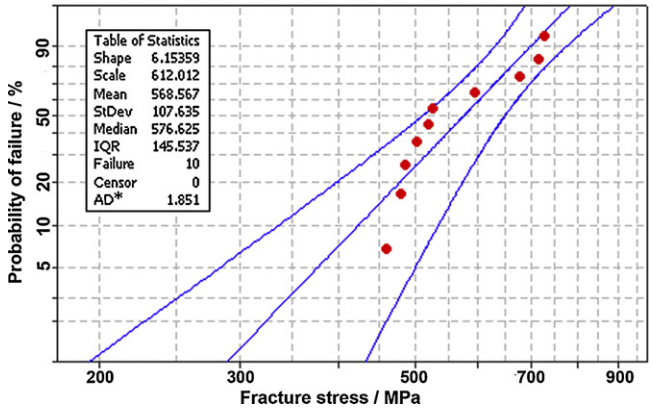


Fig. 6. Fracture stress vs. probability of failure diagram showing the distribution of the fracture strength of slip cast specimens.

with a 95% confidence interval of [2.8–4.7]. The effective volume was $V_{eff,DIP} = 7.1\ mm^3$ according to Eq. (3). Considering a fracture stress >1000 MPa of several specimens and knowing that the maximum tensile stress was ~340 MPa in the FE simulation, it can be said that DIP is a promising method to produce 3Y-TZP dental restorations. The comparatively low Weibull modulus indicates that the DIP process has to be further optimised to achieve higher reliability.

Slip casting, which is also a suspension based process, was used to produce similar bending samples for a comparative analysis of the mechanical performance of DIP components. The probability of failure diagram of the slip cast specimens is given in Fig. 6. The characteristic strength was $\sigma_{0,slip} = \sim 612$ MPa with a 95% confidence interval of [550–681]. The fracture stress values varied between ~450 MPa and ~750 MPa and a Weibull modulus was $m_{slip} = 6.2$ with a 95% confidence interval of [3.8–9.9]. Using Eq. (3) the effective volume was calculated as $V_{eff,slip} = 14.1\ mm^3$.

Remembering that the slip cast specimens had a larger volume than the DIP specimens, Eq. (4) can be applied to scale the characteristic strength of the slip cast specimens for the dimensions of the DIP produced specimens. If specimens of 1.5 mm × 3.0 mm × 30.0 mm (volume of the DIP produced specimens) were produced by slip casting, the scaled characteristic strength would be $\sigma_{0,slip,scaled} = \sim 684$ MPa, which is larger than the original $\sigma_{0,slip}$. The value of the $\sigma_{0,slip,scaled}$ is lower than the $\sigma_{0,DIP} = \sim 843$ MPa of the DIP specimens. Scaling the $\sigma_{0,DIP}$ for specimens with the dimensions of the slip cast specimens results in a $\sigma_{0,DIP,scaled} = \sim 698$ MPa, which is larger than the $\sigma_{0,slip}$. In both cases the characteristic strength of the DIP produced components is higher. As a result, it can be concluded that the DIP method is superior to the conventional slip casting method in terms of mechanical properties of the components produced.

A fractographical analysis of the tested DIP produced specimens is provided in other studies.[14,32]

## 4. Conclusions

The potentials of the direct inkjet printing (DIP) method to manufacture all-ceramic dental restorations were investigated and the following conclusions were drawn:

- 3Y-TZP as well as carbon components in millimetre scale can be produced by the DIP method.
- The DIP fabricated ceramic components reveal a smooth surface without the stair steps effect and drying or sintering cracks.
- A relative density of >96% of the theoretical density can be achieved by the DIP method.
- According to a simplified FEA study the maximum tensile stress on a dental framework would be ~340 MPa under realistic clenching conditions.
- 3Y-TZP components produced by DIP reveal a higher flexural strength (~843 MPa) than slip cast 3Y-TZP components (~684 MPa) according to the four-point bending test.

- The DIP method is a potential and promising fabrication technique for manufacturing 3Y-TZP dental restorations.

The focus of the future work must be on further optimisation of the DIP process to improve the reliability as well as the Weibull modulus of the produced components in terms of flexural strength. The ink and printing stability should be improved by the introduction of high energy milling systems or optimised additive systems. On the other hand the printing system must be further improved to enable a multi-printhead operation. Besides the printheads should be able to move in an additional *y*-axis in order to cover a larger printable area and produce larger components. Furthermore the development of specific printing software to satisfy the nozzle cleaning and deposit drying requirements is inevitable for a stable printing process.

## Acknowledgements

The authors gratefully acknowledge Heraeus Kulzer GmbH (Hanau, Germany) for supplying the special slicing software and the STL-file of the dental framework model used in this study, as well as Mr. Atılım Eser and Mr. Utku Özden (Institute for Materials Applications in Mechanical Engineering, RWTH Aachen University, Germany) for their kind support in the FE-analysis.

## References

1. Höland W, Rheinberger V, Apel E, Ritzberger C, Rothbrust F, Kappert H, et al. Future perspectives of biomaterials for dental restoration. *J Eur Ceram Soc* 2009;**29**:1291–7.
2. Dakskobler A, Jevnikar P, Oblak C, Kosmac T. The processing-related fracture resistance and reliability of root posts made from Y-TZP. *J Eur Ceram Soc* 2007;**27**:1565–70.
3. Kunzelmann KH, Kern M, Pospiech P, Mehl A, Frankenberger R, Reiss B, et al. *Vollkeramik auf einen Blick*. 2nd ed. Ettlingen/Germany: AG Keramik; 2006.
4. Studart AR, Filser F, Kocher P, Gauckler LJ. In vitro lifetime of dental ceramics under cyclic loading in water. *Biomaterials* 2007;**28**:2695–705.
5. Raigrodski AJ. Contemporary materials and technologies for all-ceramic fixed partial dentures: a review of the literature. *J Prosthet Dent* 2004;**92**(6):557–62.
6. Denry I, Kelly JR. State of the art of zirconia for dental applications. *Dent Mater* 2008;**24**:299–307.
7. Yilmaz H, Aydin C, Gul BE. Flexural strength and fracture toughness of dental core ceramics. *J Prosthet Dent* 2007;**98**(2):120–8.
8. Raigrodski AJ, Chiche GJ, Potiket N, Hochstedler JL, Mohamed SE, Billiot S, et al. The efficacy of posterior three-unit zirconium-oxide-based ceramic fixed partial dental prostheses: a prospective clinical pilot study. *J Prosthet Dent* 2006;**96**(4):237–44.
9. Filser F, Lüthy H, Schärer P, Gauckler L. In: Speidel MO, Uggowitzer PJ, editors. *All-ceramic dental bridges by Direct Ceramic Machining (DCM). Materials in Medicine, Materials Day, Department of Materials*. ETH Zürich: vdf Hochschulverlag AG; 1998. p. 165–89.
10. Filser F, Lüthy H, Schärer P, Gauckler LJ. Net-shaping of ceramic dental restorations by the Direct Ceramic Machining (DCM). In: Vincenzini P, editor. *Proceedings of CIMTEC 2002 – Advances in Science and Technology*. 2003. p. 899–906.
11. Tsumita M, Kokubo Y, von Steyern PV, Fukushima S. Effect of framework shape on the fracture strength of implant-supported all-ceramic fixed partial dentures in the molar region. *J Prosthodont* 2008;**17**:274–85.
12. Att W, Komine F, Gerds T, Strub JR. Marginal adaptation of three different zirconium dioxide three-unit fixed dental prostheses. *J Prosthet Dent* 2009;**101**(4):239–47.
13. Conrad HJ, Seong WJ, Pesun IJ. Current ceramic materials and systems with clinical recommendations: a systematic review. *J Prosthet Dent* 2007;**98**(5):389–404.
14. Ebert J, Özkol E, Zeichner A, Uibel K, Weiss Ö, Koops U, et al. Direct inkjet printing of dental prostheses made of zirconia. *J Dent Res* 2009;**88**(7): 673–6.
15. Tay BY, Evans JRG, Edirisinghe MJ. Solid freeform fabrication of ceramics. *Int Mater Rev* 2003;**48**:341–70.
16. Calvert P, Crockett R. Chemical solid free-form fabrication: making shapes without molds. *Chem Mater* 1997;**9**:650–63.
17. Lewis JA, Gratson MG. Direct writing in three dimensions. *Mater Today* 2004;**7**:32–9.
18. Chartier T, Chaput C, Doreau F, Loiseau M. Stereolithography of structural complex ceramic parts. *J Mater Sci* 2002;**37**:3141–7.
19. Silva NRFA, Witek L, Coelho PG, Thomson VP, Rekow ED, Smay J. Additive CAD/CAM process for dental prostheses. *J Prosthodont* 2011;**20**:93–6.
20. Wang J, Shaw LL, Cameron TB. Solid freeform fabrication of permanent dental restorations via slurry micro-extrusion. *J Am Ceram Soc* 2005;**89**(1):346–9.
21. Michna S, Wu W, Lewis JA. Concentrated hydroxyapatite inks for direct-write assembly of 3D periodic scaffolds. *Biomaterials* 2005;**26**: 5632–9.
22. Lewis JA, Smay JA, Stuecker J, Cesarano III J. Direct ink writing of three-dimensional ceramic structures. *J Am Ceram Soc* 2006;**89**(12):3599–609.
23. Bourell DL, Marcus HL, Barlow JW, Beamann JJ. Selective laser sintering of metals and ceramics. *Int J Powder Metall* 1992;**28**:369–81.
24. Griffin C, Danfenbach J, McMillin S. Desktop manufacturing: LOM vs. pressing. *Bull Am Ceram Soc* 1994;**73**:109–13.
25. Sachs EM, Cima MJ, Williams P, Brancazio D, Cornie J. Three-dimensional printing: rapid tooling and prototypes directly from a CAD model. *J Eng Ind* 1992;**114**:481–8.
26. Bergmann C, Lindner M, Zhang W, Koczur K, Kirsten A, Telle R, et al. 3D printing of bone substitute implants using calcium phosphate and bioactive glasses. *J Eur Ceram Soc* 2010;**30**(12):2563–7.
27. Zhao X, Evans JRG, Edirisinghe MJ, Song JH. Ink-jet printing of ceramic pillar arrays. *J Mater Sci* 2002;**37**:1987–92.
28. Derby B, Reis N. Inkjet printing of highly loaded particulate suspensions. *MRS Bull* 2003;**28**:815–8.
29. Lejeune M, Chartier T, Dossou-Yovo C, Noguera R. Ink-jet printing of ceramic micro pillar arrays. *J Eur Ceram Soc* 2009;**29**:905–11.
30. Cappi B, Ebert J, Telle R. Rheological properties of aqueous $Si_3N_4$ and $MoSi_2$ suspensions tailor-made for direct inkjet printing. *J Am Ceram Soc* 2011;**94**:111–6.
31. Özkol E, Ebert J, Uibel K, Wätjen AM, Telle R. Development of high solid content aqueous 3Y-TZP suspensions for direct inkjet printing using a thermal inkjet printer. *J Eur Ceram Soc* 2009;**29**(3):403–9.
32. Özkol E, Wätjen AM, Bermejo R, Deluca M, Ebert J, Danzer R, et al. Mechanical characterisation of miniaturised direct inkjet printed 3Y-TZP specimens for microelectronic applications. *J Eur Ceram Soc* 2010;**30**:3145–52.
33. Cappi B, Özkol E, Ebert J, Telle R. Direct inkjet printing of $Si_3N_4$: characterization of ink, green bodies and microstructure. *J Eur Ceram Soc* 2008;**28**(13):2625–8.
34. Mott M, Evans JRG. Zirconia/alumina functionally graded material made by ceramic ink jet printing. *Mater Sci Eng* 1999;**271**(A):344–52.
35. Mott M, Song JH, Evans JRG. Microengineering of ceramics by direct ink-jet printing. *J Am Ceram Soc* 1999;**82**(7):1653–8.
36. Derby B. Inkjet printing ceramics: from drops to solid. *J Eur Ceram Soc* 2011;**31**(14):2543–50.
37. Kumagai H, Suzuki T, Hamada T, Sondang P, Fujitani M, Nikawa H. Occlusal force distribution on the dental arch during various levels of clenching. *J Oral Rehabil* 1999;**26**:932–5.
38. Lee JH, Song YB. A study on maximum occlusal force of Korean adults with normal occlusion according to cephalometric measurements. *Ajou Med J* 1997;**2**(1):67–77.

39. Dourandish M, Simchi A. Study the sintering behavior of nanocrystalline 3Y-TZP/430L stainless-steel composite layers for co-powder injection molding. *J Mater Sci* 2009;**44**:1264–74.
40. Iramaneerat K, Hlsano M, Soma K. Dynamic analysis for clarifying occlusal force transmission during orthodentic archwire application: difference between ISW and stainless steel wire. *J Med Dent Sci* 2004;**51**:59–65.
41. Ausiello P, Rengo S, Davidson CL, Watts DC. Stress distributions in adhesively cemented ceramic and resin-composite Class II inlay restorations: a 3D-FEA study. *Dent Mater* 2004;**20**:862–72.
42. Özkol E, Ebert J, Telle R. An experimental analysis of the influence of the ink properties on the drop formation for direct thermal inkjet printing of high solid content aqueous 3Y-TZP suspensions. *J Eur Ceram Soc* 2010;**30**(7):1669–78.
43. Frischholz P. *The Breviary Technical Ceramics*. 4th ed. Selb/Germany: Fahner Verlag; 2004 [chapter 5].
44. Quinn GD. Weibull strength scaling for standardized rectangular flexure specimens. *J Am Ceram Soc* 2003;**86**(3):508–10.